

# STRUCTURAL ANALYSIS OF CONCRETE PRE-STRESSED RESERVOIRS FOR SLUDGE FERMENTATION – WASTE WATER TREATMENT PLANT BUCHAREST – GLINA.

## NUMERICAL FEM ASSESSMENT OF THE DYNAMIC STRUCTURAL RESPONSE

**Tudor BUGNARIU** – Professor, PhD, Technical University of Civil Engineering Bucharest, Faculty of Hydrotechnics, e-mail: bugnariu@utcb.ro

**Abstract:** The paper refers to a structural finite element analysis on the reservoirs for sludge fermentation at Glina Waste Water Treatment Plant. The purpose was to assess the dynamic response of the structure, the stress and deformation states due to the design earthquake. A linear-elastic analysis was performed, according to the Romanian actual codes, in order to verify the design provisions and to emphasize the sensitivities, for a structure which was designed by analytical procedures. The results obtained on the numerical models highlight the importance of the soil-structure interaction, in peculiar the one influenced by the soil mass deformability, on the overall structural response. Based on the results of the analysis, an in-situ measurement campaign for structural dynamic characteristics was initiated, taking advantage of the ongoing repair works with subsequent exhaustion and re-filling of reservoir No. 4.

**Keywords:** numerical modeling, modal and spectrum analysis, soil-structure interaction

### 1. Introduction

This paper resumes the presentation of modeling procedures and results concerning the structural analysis and soil-structure interaction of the sludge fermentation reservoir' at Glina waste water treatment plant. The first part, dedicated to static analysis, was presented before in the same journal, Vol. 9 No. 1 – 2013. Information regarding the design data, FE models, concrete pre-stressing simulation, calibration, were given at large in the first part of the study. The dynamic analysis was performed basically on the same structural models, being modified and adapted according to specific needs.

The dynamic response of the structure, defined by its own vibration modes and shapes, as well as the spectrum analysis, was analyzed on the numerical model considered base-embedded (with constrained foundation slab). The complete soil-structure assembly was used only for the equivalent static analysis.

### 2. Structural design data

The reservoirs for sludge fermentation are civil engineering structures made in reinforced pre-stressed concrete with post-tensioned reinforcement. The reservoir's shape was designed to satisfy the technological requirements for the fermentation process as well the optimization of its structural behavior. The result is a special axial-symmetrical volume, made of thin plates with toroidal, tapered and cylindrical shapes. The internal geometry provides a satisfactory hydraulic spectrum for the sludge recirculation, an external surface close to minimum and an advantageous behavior for static and dynamic loads.

Information concerning the geotechnical characteristics of the ground were limited when the analysis was done, but according to the design provisions, the foundation slab is placed over a 1.5 m thick sand and gravel layer, replacing the deformable natural clayey/dusty ground

encountered down to the depth of 5 m. Below, the natural ground is made of sandy and sand and fine gravel layers with medium boulders, down to a depth of 18 m. The ground water level was intercepted at a depth of 4.5 m. A sketch of the structure is provided in the previous paper.

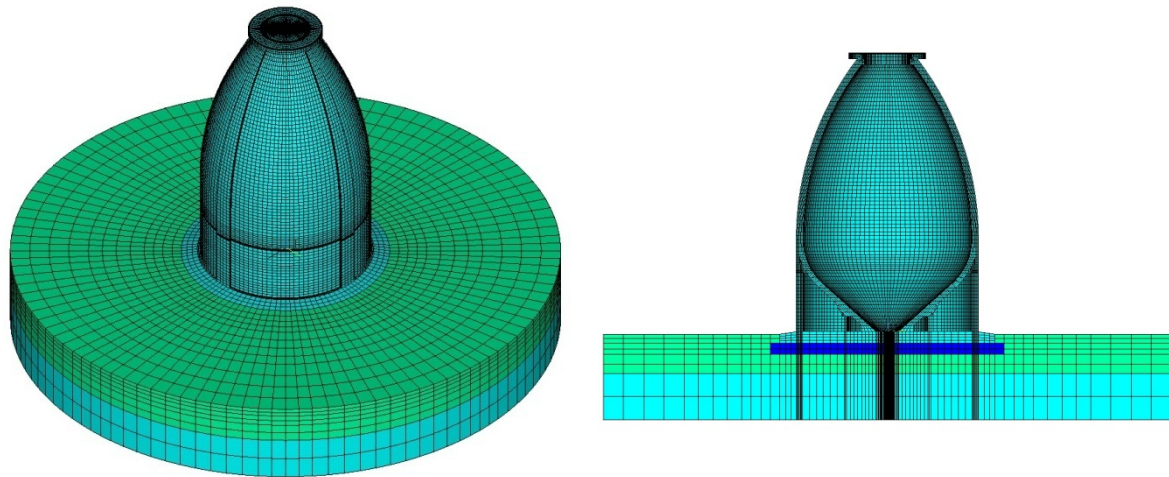


**Fig. 1** - Axonometric view and vertical cross section of the FE model

### **3. Stages of dynamic analysis**

According to its objectives, the dynamic analysis followed the subsequent stages:

- a) Modal analysis, extracting a significant number of own vibration modes (shapes and frequencies), on empty and filled-up reservoir.
- b) Spectrum analysis. The design spectra were chosen according to the Romanian design codes P100/2006 and P100/2013.
- c) Combination of static load effects (common in-duty loads) with the results of the spectrum analysis [STATIC  $\pm$  SPECTRUM].
- d) Drawing out from the spectrum analysis the amplification characteristics of the response expressed in horizontal accelerations and the vertical distribution of inertia forces, respectively; appropriate modification of the FE model.
- e) The static – equivalent analysis with horizontal inertia loads.
- f) Effect combination, due to common in-duty loads with the results of the static – equivalent analysis [STATIC  $\pm$  STATIC EQUIVALENT].

For all the above analysis stages, the model is assumed to pay linear-elastic behavior, cumulative effects of load cases being permitted.

### **4. Interaction between Structure and Sludge Mass**

The specific structural design refers to stress and displacement fields under the maximum values of the hydro-dynamic pressure. The structural response of a reservoir can be framed into one of the following categories:

- The response in accelerations, when the fluid-reservoir assembly behaves like a rigid system, the fluid mass being one with the structure;
- The response in displacements, when the fluid-reservoir assembly behaves like independent components; the fluid reveals low frequency oscillations and low damping (a quasi sinusoidal response).

According to the European design code EN 1998 - 4:2006 and the engineering practice, the earthquake design of reservoirs applies to splitting the response components, with different approaches.

In case of the response in accelerations, the fluid mass has the same accelerations and displacements as the structure does. The earthquake effect is dominated by the inertia loads related to both components. In case of the response in displacements, the fluid mass oscillates inside the reservoir, inducing high hydro-dynamic pressures on the reservoir walls. The weight of each type of response can be assessed invoking a simplified approach. The total fluid mass  $M$  is replaced by two equivalent masses,  $M_0$  and  $M_1$ . The mass  $M_0$  stands for the response component in accelerations and is “glued” to the reservoir. The mass  $M_1$  stands for the response component in displacements and is attached to the reservoir by two springs, with equivalent stiffness of the fluid mass oscillation. Each mass is subjected to inertia loads  $c \times g \times M_0$  and  $c \times g \times M_1$ , where  $c$  is the seismic coefficient. The equivalent masses are:

$$M_0 = \frac{\text{th}(1.7R/H)}{1.7R/H} M$$

$$M_1 = \frac{0.71 \text{th}(1.8H/R)}{1.8H/R} M$$

with  $R$  the reservoir radius and  $H$  the fluid height inside the reservoir.

Replacing the mean value of radius  $R = 7$  m and the height  $H = 36$  m, the equivalent masses yield  $M_0 = 0.967M$  and  $M_1 = 0.0901M$ . Hence, for the dynamic analysis, the sludge mass was considered “glued” with the reservoir. The option is also justified by the fact that, in common in-duty conditions, the reservoir is filled-up to elevation +34.50 m, no space being available for fluid oscillations (sloshing effect).

## 5. Modal Analysis

The modal analysis is performed on the structural model embedded at the bottom of the foundation slab. This approach is justified by the relative high deformability of the foundation ground, which roughly modifies the dynamic response of the assembly. The modal analysis was performed on both empty and filled-up reservoir conditions.

The mass characteristics of the model are given by:

- the own mass of the structure, by assigning the solid elements density;
- the additional masses, attached to the nodes placed on the inner surface of the reservoir, to catch the contribution of the contained sludge to the own vibration frequencies.

The stiffness characteristics of the model are given by the elasticity modulus assigned for concrete. The preliminary test revealed that the pre-stressing fascicles have little influence over the dynamic response, thus the pre-stressing effect was neglected. The elasticity modulus was assigned equal to the one used in static analyses (at least till the calibration in the field measurements will be finalized), due to the following conflicting reasons:

- usually, the dynamic modulus is higher;
- the lower cylindrical plates of the reservoir, with passive reinforcement (and no pre-stressing) may exhibit some post-elastic behavior in case of strong dynamic loads, diminishing the modulus value.

### 6. Additional Masses

The additional masses, connected to nodes placed on the inner surface of the reservoir, were assessed by dividing the total sludge volume into 19 partial volumes, along the elevation. Each mass was again divided by the number of available nodes corresponding to the partial volume. The discrete vertical distribution of masses is represented in figure 2. A total number of 8390 concentrated mass elements were defined between elevations ±0.00 and +35.30. The additional mass distribution is summarized in the adjoining table.

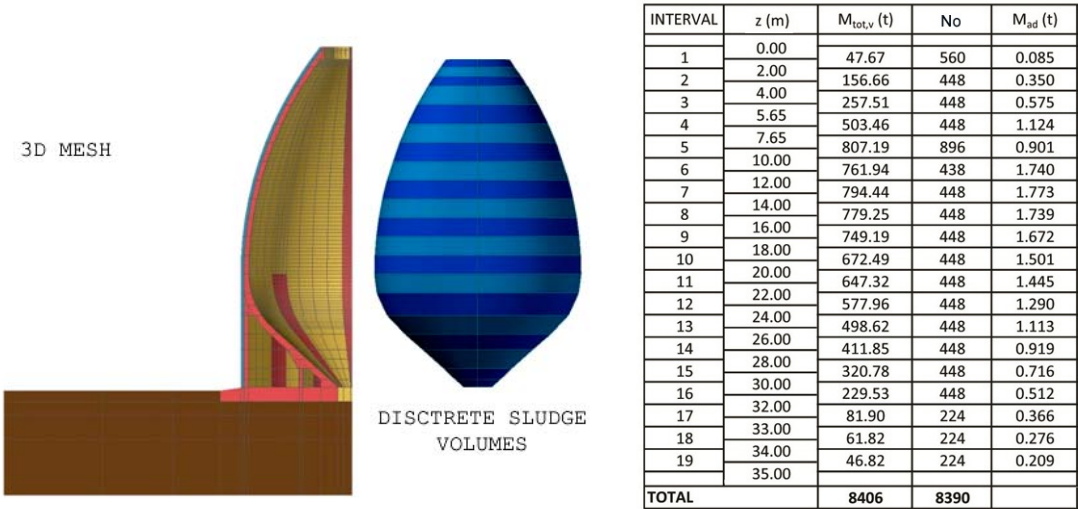


Fig. 2 – Additional mass evaluation. Discrete sludge volumes. Assigned mass values.

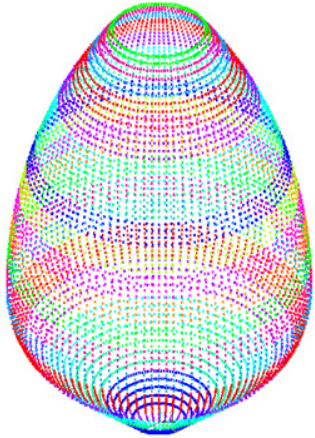


Fig. 3 – Concentrated mass elements attached to nodes on the inside face of the reservoir.

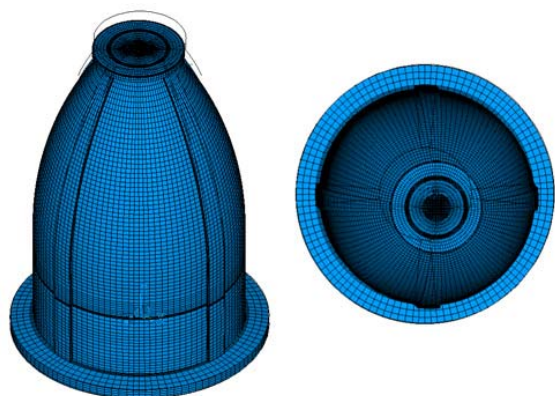
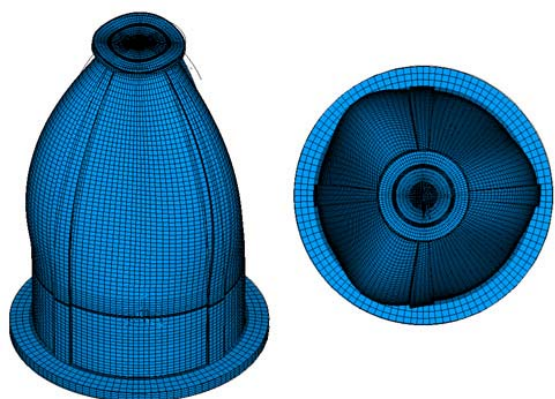
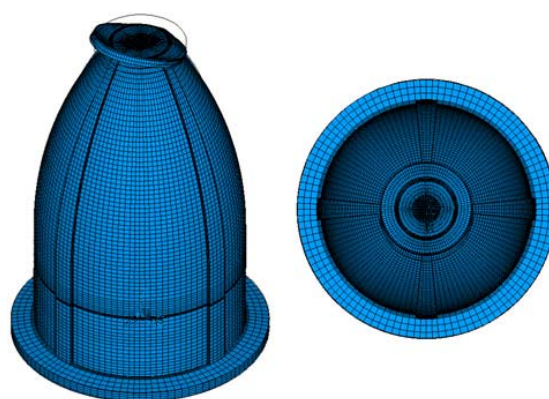
### 7. Modal Analysis Results

For both the empty and the filled-up reservoir, the first 10 vibration modes were considered. Due to the double symmetry of the model, the pairs of vibration modes have almost identical frequencies and shapes, as a result of numerical approximation.

For the empty reservoir, the first natural frequency is  $F_1 = 9.798$  Hz (corresponding to a natural period of  $T_1 = 0.102$  sec), while the vibration shape in the first mode represents a balance by translation along an oblique direction (between the meridian stiffeners) oriented at 21 degrees from the x axis. The frequencies for the first 10 vibration modes are given in table 1. The representations of the vibration shapes reveal that the modes 3, 4, 5, 8, 9, 10 do not affect the main structure, but only the upper cantilever plate (figures 4 – 6). The results on the empty reservoir are used only for comparison with those obtained in filled-up conditions and for later calibration of the model (with the in-situ frequency measurements).

Natural vibration frequencies for empty reservoir

VIBRATION MODE	FREQUENCY	PERIOD
	(Hz)	(sec)
1	9.798	0.102
2	9.798	0.102
3	16.698	0.060
4	17.530	0.057
5	18.572	0.054
6	19.850	0.050
7	19.850	0.050
8	19.937	0.050
9	21.098	0.047
10	21.098	0.047

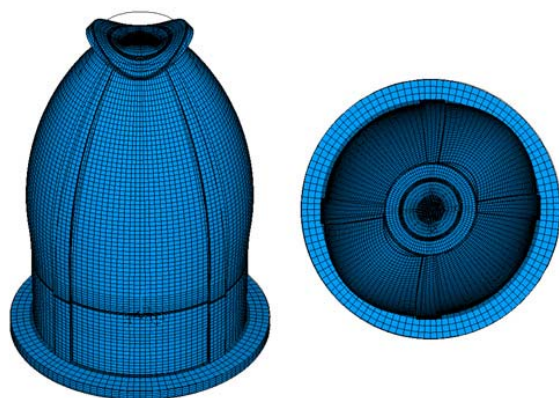
Fig. 4 – 1<sup>st</sup> natural vibration shapeFig. 5 – 6<sup>th</sup> natural vibration shapeFig. 6 – 9<sup>th</sup> natural vibration shape

The modal analysis performed on the filled-up reservoir yield the results given in table 2. The first vibration frequency is  $F_1 = 5.214$  Hz (a fundamental period of  $T_1 = 0.192$  sec), with the same vibration shape as for the empty reservoir. The presence of additional masses does not affect only the natural frequencies, but also the vibration shapes, emphasizing the deformation of the reservoir itself, including general torsion. Some examples are represented in figures 7 – 9.

Table 2

Natural vibration frequencies for filled-up reservoir

VIBRATION MODE	FREQUENCY	PERIOD
	(Hz)	(sec)
1	5.214	0.192
2	5.215	0.192
3	8.383	0.119
4	8.855	0.113
5	9.296	0.108
6	9.297	0.108
7	10.278	0.097
8	10.617	0.094
9	11.322	0.088
10	12.400	0.081

Fig. 7 – 3<sup>rd</sup> natural vibration shape

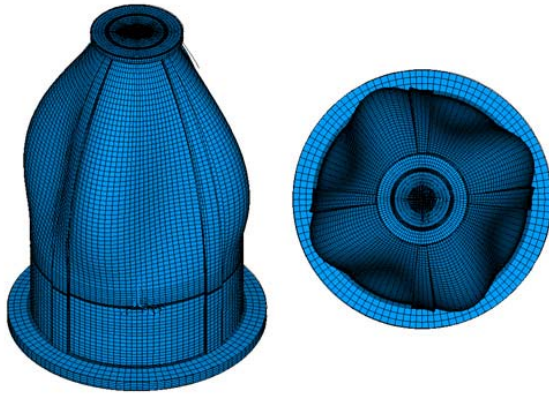


Fig. 8 – 7<sup>th</sup> natural vibration shape

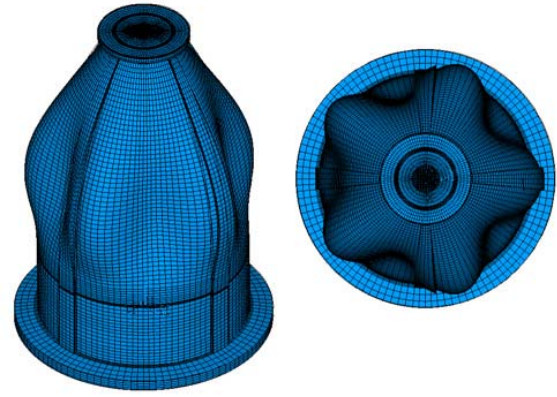


Fig. 9 – 10<sup>th</sup> natural vibration shape

## 8. Spectrum Analysis

This analysis is based on the results of the modal analysis carried out on the filled-up reservoir. The embedded structural model was used.

## 9. Response Spectra

The elastic response spectra for the reservoir location ( $T_C = 1.6$  sec,  $\xi = 5\%$ ) are considered according to the Romanian design codes P100/2006 and P100/2013. The difference is made by the maximum value of the amplification factor  $\beta(T)$  and the corner period  $T_B$ . According to the fundamental period, the maximum amplification corresponds to the former design code P100/2006, thus only these results will be represented (all the more, no significant differences were noticed).

For the design spectra, the reservoir was framed into class II ( $\gamma_I = 1.2$ ), as for the structural behavior coefficient  $q$ , according to EN-1998-4:2006, for concrete fluid tanks, the maximum value is  $q = 1.5$ . The option is justified also by the fact that most of the structure is presumed to remain in linear-elastic state. The maximum ground acceleration on site is  $a_g = 0.24g = 2.354$  m/s<sup>2</sup> (P100/2006) or  $a_g = 0.30g = 2.943$  m/s<sup>2</sup> (P100/2013).

The elastic and design response spectra are represented in figures 10.a and 10b. The yielding maximum accelerations differ ( $a_{max} = 5.18$  m/s<sup>2</sup> and  $a_{max} = 5.88$  m/s<sup>2</sup>), but the spectral value related to the fundamental period is larger for P100/2006. An abstract of the spectrum analysis for the design code P100/2006 is given in table 3. For both spectra the essential contribution of the first vibration mode is evident, with an involved mass fraction of almost 95%.

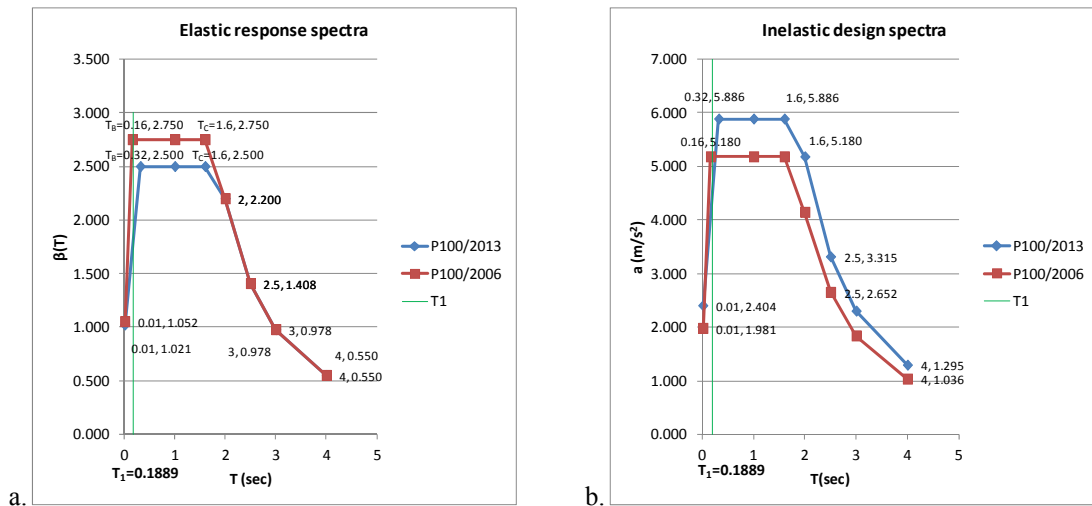


Fig. 10 – Elastic and design spectra according to the design codes P100/2006 and P100/2013.

The stress and deformation state (combining the first 10 modes) is exclusively due to the seismic action (no gravity loads considered). The deformed shape indicates a global displacement with two components ( $u_{y,max} = 7.28 \text{ mm}$  and  $u_{x,max} = 2.69 \text{ mm}$ ), the larger one along the direction of the applied spectrum.

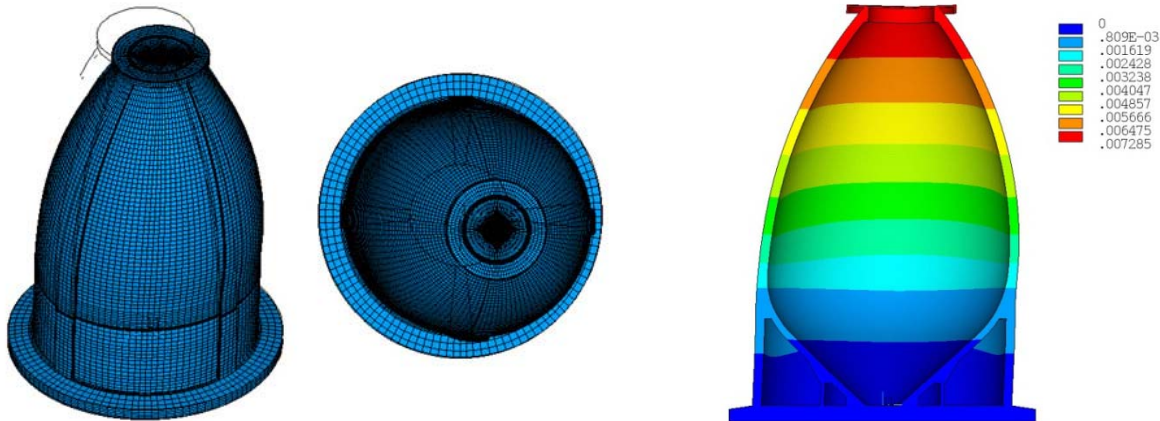


Fig. 11 – Deformed shape and horizontal displacement distribution  $u_y$  (m) for **SPECTRUM Y** analysis.

The stress values have no other significance but as relative values, overlapped on the actual in-duty state of stress. However, graphical representations emphasize that similar level of stress yields for both spectra and any applying direction. Some results are represented in figures 12 and 13.

Both stress and displacement results of the spectrum analysis should be combined with those of a static analysis, performed on the same model. The load cases are combined in the following [STATIC]+[SPECTRUM] and [STATIC]-[SPECTRUM] solutions, to emphasize the envelope of maximum stresses.

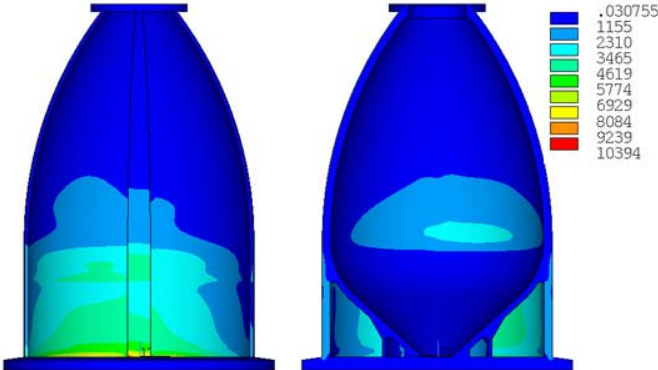


Fig. 12 – Spectrum analysis. **SPECTRUM Y** - Vertical stress distribution  $\sigma_z$  (KN/m<sup>2</sup>).

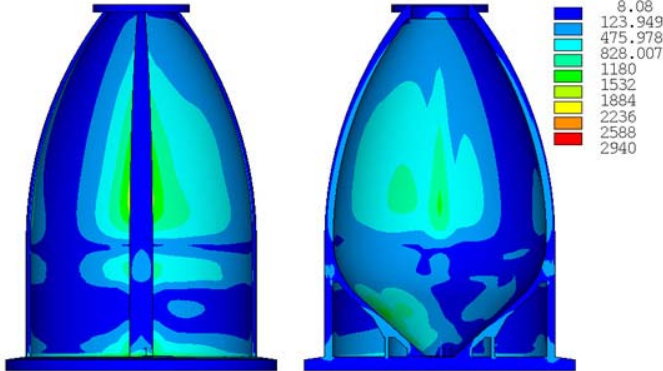
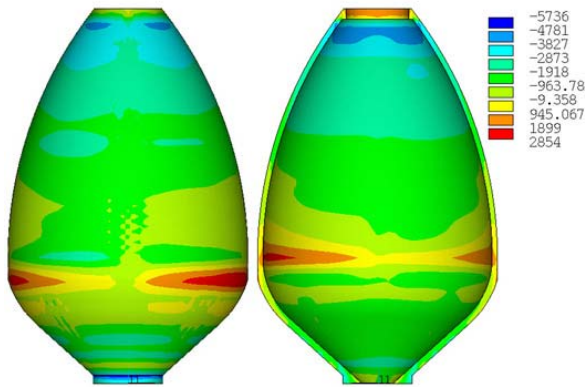
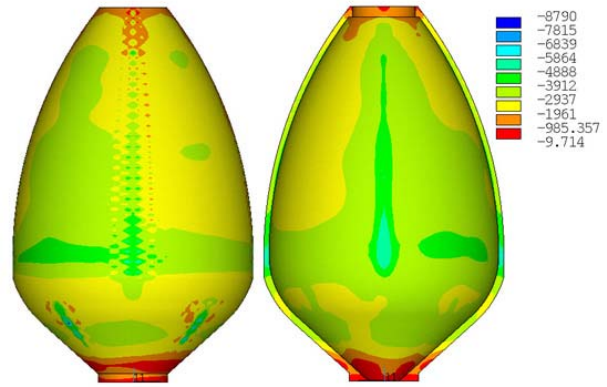


Fig. 13 – Spectrum analysis. **SPECTRUM Y** - Ring stress distribution  $\sigma_\theta$  (KN/m<sup>2</sup>).

Results of stress distribution are picked-up for separated structural components and represented in figures 14 – 17.



**Fig. 14** – Combination ST+SPECX – Vertical stress distribution  $\sigma_z$  (KN/m<sup>2</sup>)



**Fig. 15** – Combination ST+SPECX – Ring stress distribution  $\sigma_\theta$  (KN/m<sup>2</sup>)

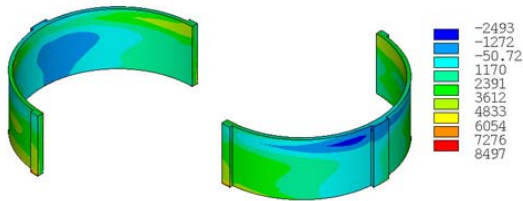


**Fig. 16** – Combination ST + SPECX – Vertical stress distribution  $\sigma_z$  (KN/m<sup>2</sup>)

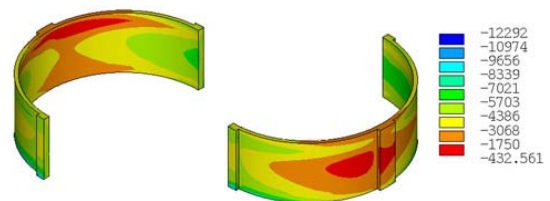


**Fig. 17** – Combination ST – SPECX – Vertical stress distribution  $\sigma_z$  (KN/m<sup>2</sup>)

Based on the same spectrum analysis, the distribution of horizontal acceleration calculated in all nodal points of the mesh becomes available. The distribution of total acceleration  $a_{sum}$  represented in figure 18 emphasizes the dynamic amplification effect along the vertical axis.

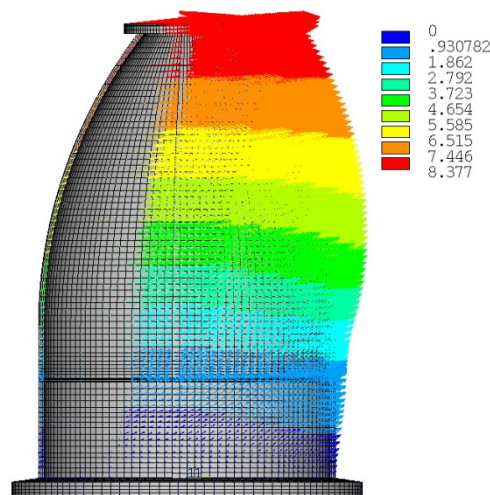


**Fig. 18** – Vertical distribution of nodal acceleration (m/s<sup>2</sup>).

## 10. Remarks on Results of Spectrum Analysis

The stress concentrations are located at the base of the cylindrical plates, at the connection with the foundation slab, and at the interface between the toroidal plates and the meridian stiffeners. A sensitive region is also the one joining the inferior tapered and toroidal plates. Maximum vertical tensions up to 6500 KN/m<sup>2</sup> occur in the [STATIC + SPECTUM] combination at the base of the

cylindrical plate (outside) and at its embedment into the stiff ring at elevation +12.00 (inside). Along the ring direction ( $\theta$ ) most of the structure remains in compression, except the base of the exterior cylindrical plate. The maximum ring stresses are locally concentrated near-by the meridian stiffeners, where the pre-stressing fascicules are attached, but they are comparable to those drawn out from the static analysis.

For the [STATIC - SPECTRUM] combination, vertical tensions occur only at the foundation slab and the upper horizontal ring at elevation +36.00. Otherwise, the structure remains in compression with maximum stresses up to  $-10600 \text{ KN/m}^2$ . The ring stress values are similar to those obtained in the first combination.

Concerning the restricted area of the container itself, the vertical stresses due to combination 1 are mostly compressions, except the stiff ring at elevation +12.00, where tensions up to  $2850 \text{ KN/m}^2$  occur on both faces. On ring direction ( $\theta$ ), the reservoir structure remains in compression, with no less than  $-10 \text{ KN/m}^2$ . For combination 2, the vertical tensions move to the upper ring at elevation +36.00, all the other components resting in compression. Along the ring direction only the compressions are present, with a maximum value of  $-7200 \text{ KN/m}^2$ .

**11. Static Equivalent Analysis**

For modeling purposes, where the structural response is expressed in displacements and stresses preserving their real sign, a static equivalent analysis was performed. The main advantages are:

- results are more relevant and intuitive for engineering interpretation;
- the complete model, involving the ground – structure assembly is analyzed.

The method facilitates getting results on the mutual interaction and interface stresses between the ground and the foundation slab, emphasizes the influence of the ground deformability and makes possible the assessment of settlements, stresses and deformations of the foundation slab. The static equivalent analysis is based on the processed results of the spectrum analysis, modeling the amplification effect and applying horizontal inertia forces, with variable vertical distribution.

**12. Discrete distribution of acceleration**

The values of nodal accelerations, available after performing the spectrum analysis, are grouped in successive intervals, corresponding to the additional masses with the same value. For each interval, the acceleration was averaged over the selected set of nodes. The post-processing of nodal accelerations yield into the discrete distribution shown in figure 19 and the adjoining table.

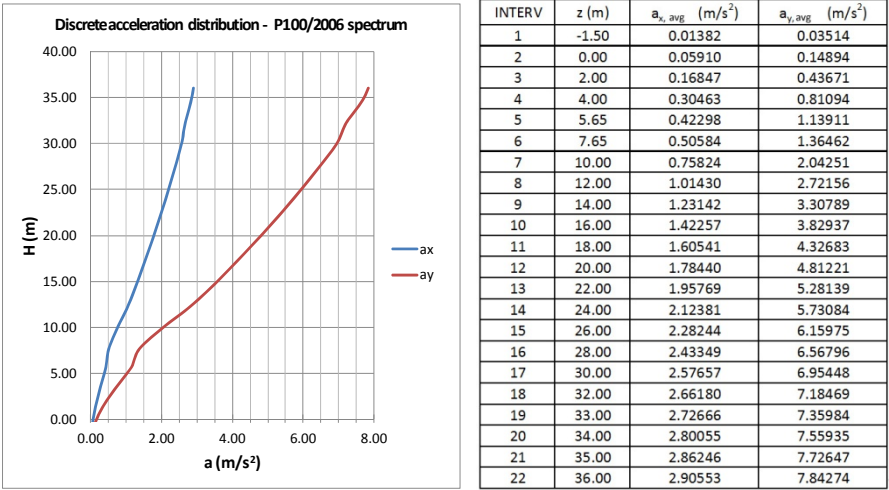


**Fig. 19** – Vertical distribution of discrete acceleration (m/s<sup>2</sup>). Average acceleration table.

The total vibrating mass, made of the structure itself and the contained sludge, was divided into the same intervals by horizontal planes. The local masses of the structure correspond to each delimited concrete volume, as it was shown before. The discrete vertical distribution of the masses is represented in figure 20.

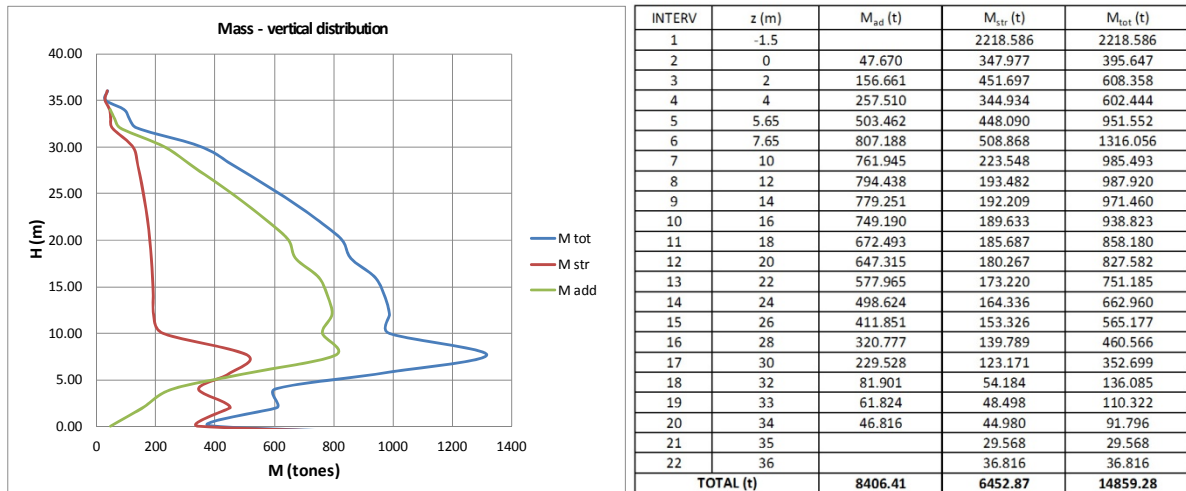


Fig. 20 – Vertical distribution of masses (tonnes). Table with total mass components.

The discrete inertia forces, as multiplication between the discrete masses and the discrete response accelerations, are shown in figure 21 and listed in the adjoining table.

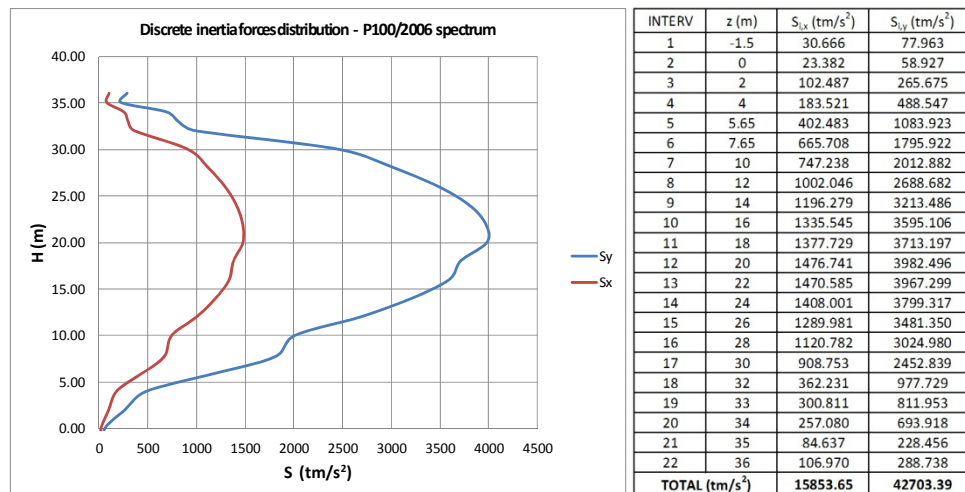


Fig. 21 – Discrete inertia forces distribution. Results for P100/2006 spectrum.

The total value represents the base shear force on each direction. Dividing the base shear force by the total weight of the structure–sludge assembly, the global seismic coefficients yield on each direction:

$$c_x = 0.11$$

$$c_y = 0.29$$

In the framework of the static equivalent method, a unique acceleration value is applied at all constrained nodes of the finite element model (at the bottom of the slab, for the analysis concerning the structure only, and over the lateral and bottom limits of the soil mass, for the complete model). This corresponds to the single point response spectrum used in the spectrum analysis. Thus, in order to keep the same vertical distribution of inertia loads for a unique value of ground acceleration (0.24g/0.30g), the discrete mass distribution was corrected by dividing the inertia force on each interval by the constant acceleration value. The additional masses were reassigned for each interval, while for the structure, the mass modification was performed by modifying the local density. The mass correction procedure was organized as spreadsheets, shown in figure 22.

	z (m)	a <sub>y</sub> (m/s <sup>2</sup> )	S <sub>ky</sub> (tm/s <sup>2</sup> )	M (t)	M <sub>add</sub> coef	M <sub>str</sub> coef	modif M <sub>add</sub> (t)	modif M <sub>str</sub> (t)	M <sub>ad</sub> No.	modif M <sub>add</sub> (t)	V (m <sup>3</sup> )	ρ (t/m <sup>3</sup> )
1	-1.5	2.354	77.963	33.114		1.000		33.114			887.434	0.037
2	0	2.354	58.927	25.028	0.120	0.880	3.016	22.013	560.000	0.005	139.191	0.158
3	2	2.354	265.675	112.842	0.258	0.742	29.058	83.783	448.000	0.065	180.679	0.464
4	4	2.354	488.547	207.504	0.427	0.573	88.696	118.808	448.000	0.198	137.974	0.861
5	5.65	2.354	1083.923	460.382	0.529	0.471	243.586	216.796	448.000	0.544	179.236	1.210
6	7.65	2.354	1795.922	762.794	0.613	0.387	467.851	294.943	896.000	0.522	203.547	1.449
7	10	2.354	2012.882	854.945	0.773	0.227	661.010	193.935	438.000	1.509	89.419	2.169
8	12	2.354	2688.682	1141.982	0.804	0.196	918.327	223.655	448.000	2.050	77.393	2.890
9	14	2.354	3213.486	1364.885	0.802	0.198	1094.835	270.050	448.000	2.444	76.884	3.512
10	16	2.354	3595.106	1526.973	0.798	0.202	1218.540	308.433	448.000	2.720	75.853	4.066
11	18	2.354	3713.197	1577.131	0.784	0.216	1235.882	341.249	448.000	2.759	74.275	4.594
12	20	2.354	3982.496	1691.512	0.782	0.218	1323.061	368.451	448.000	2.953	72.107	5.110
13	22	2.354	3967.299	1685.058	0.769	0.231	1296.490	388.567	448.000	2.894	69.288	5.608
14	24	2.354	3799.317	1613.709	0.752	0.248	1213.699	400.010	448.000	2.709	65.734	6.085
15	26	2.354	3481.350	1478.657	0.729	0.271	1077.514	401.143	448.000	2.405	61.330	6.541
16	28	2.354	3024.980	1284.820	0.696	0.304	894.857	389.963	448.000	1.997	55.916	6.974
17	30	2.354	2452.839	1041.811	0.651	0.349	677.986	363.825	448.000	1.513	49.268	7.385
18	32	2.354	977.729	415.277	0.602	0.398	249.929	165.348	224.000	1.116	21.674	7.629
19	33	2.354	811.953	344.866	0.560	0.440	193.262	151.605	224.000	0.863	19.399	7.815
20	34	2.354	693.918	294.733	0.510	0.490	150.314	144.419	224.000	0.671	17.992	8.027
21	35	2.354	228.456	97.034		1.000		97.034			11.827	8.204
22	36	2.354	288.738	122.638		1.000		122.638			14.726	8.328

Fig. 22 – The mass correction procedure

### 13. Load Case Combination for the Static Equivalent Method

The static equivalent method should consider the cumulated effect of gravity, pre-stressing, internal pressure and inertia forces. Thus, the following load cases were defined:

- STATIC [ST] – the structure subjected to its own weight, pre-stressing and internal pressure (which by default includes the weight of sludge);
- STATIC EQUIVALENT Y [EQY] – the structure subjected to horizontal inertia forces along the Y axis, according to the structural response on this direction;
- STATIC EQUIVALENT X [EQX] – the structure subjected to horizontal inertia forces along the X axis, according to the structural response on this direction.

The three load cases were joined into the following load combinations:

- Combination 1 – [ST]+[EQY]+[EQX];
- Combination 2 – [ST]-[EQY]-[EQX]

for both embedded and complete finite element models.

A few examples of results expressed in displacements and stresses over the structural assembly and its components are represented in figures 23 – 28. For the embedded model, it is obvious that the displacement field is similar to the one established in the combination with the spectrum analysis. The stress distribution also shows comparable levels of stress and concentration regions.

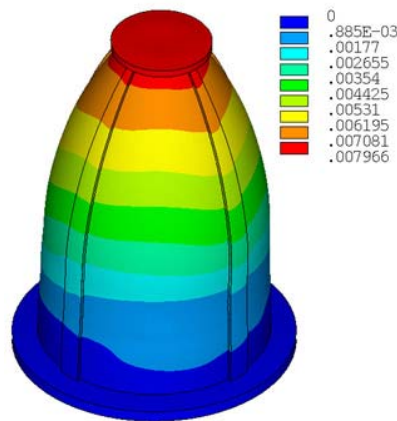


Fig. 23 – Horizontal displacement distribution  $u_{sum}$  (m) for combination [ST]-[EQY]-[EQX].

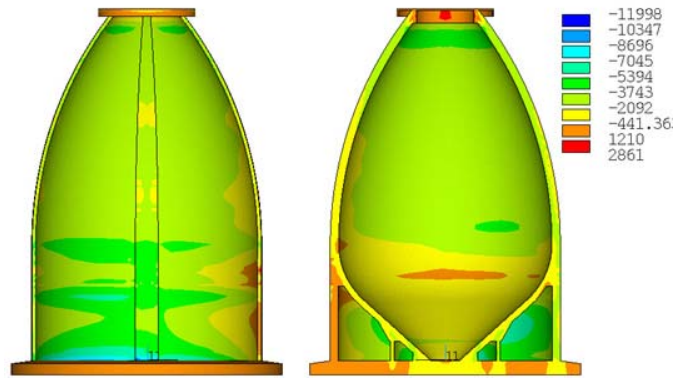


Fig. 24 – Vertical stress distribution  $\sigma_z$  for combination [ST]-[EQY]-[EQX] (KN/m<sup>2</sup>).

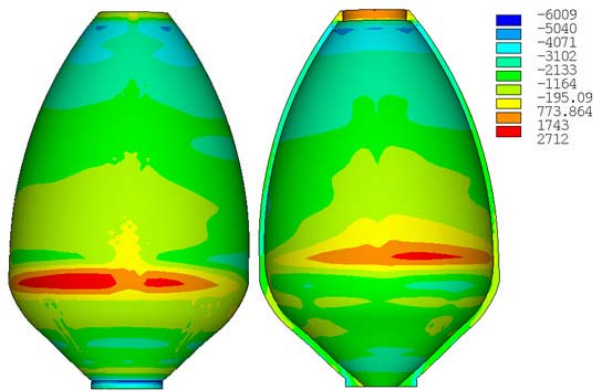


Fig. 25 – Vertical stress distribution  $\sigma_z$  for combination [ST]+[EQY]+[EQX] (KN/m<sup>2</sup>)

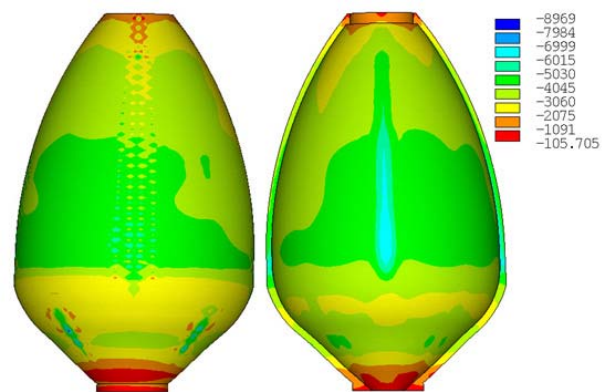


Fig. 26 – Ring stress distribution  $\sigma_\theta$  for combination [ST]+[EQY]+[EQX] (KN/m<sup>2</sup>)

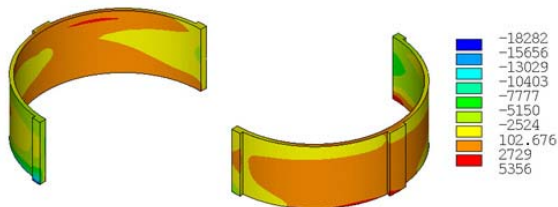


Fig. 27 – Vertical stress distribution  $\sigma_z$  for combination [ST]+[EQY]+[EQX] (KN/m<sup>2</sup>)

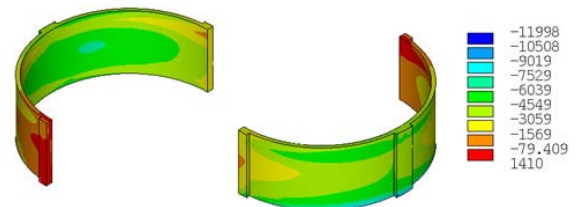


Fig. 28 – Vertical stress distribution  $\sigma_z$  for combination [ST]-[EQY]-[EQX] (KN/m<sup>2</sup>)

#### 14. Stresses and Deformation of Foundation Soil Mass

Concerning the soil mass, the result of both load case combinations are identical, due to the axial symmetry of the structure and model. The vertical displacements of the ground surface below the foundation slab have a quasi – linear distribution, emphasizing a rigid body behavior of the structure, compared with the deformed soil mass. A local detail of the deformed shape, as well as the vertical displacement graph for the selected nodes at the bottom of the foundation slab are represented in figure 29. The maximum settlement in the compressed region is about 6.7 cm, while in the opposite direction the ground level mounts for up to 1.4 cm (indicating a local detachment drift at the contact). From the point of view of contact stresses, they are framed between +100 ... -570 KN/m<sup>2</sup>, with local concentrations up to -900 KN/m<sup>2</sup>.

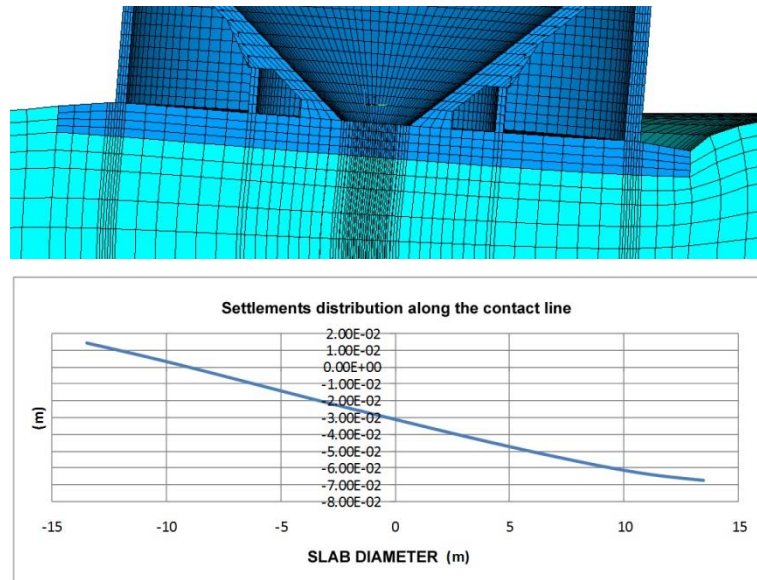


Fig. 29 – Combination [ST]–[EQY]–[EQX] – deformed shape and settlements distribution.

The positive values (tensions) are due to the model limitation, which so far does not include contact elements, permitting detachment. In fact, a redistribution of stresses occurs, with an appropriate augmentation of compression stresses. Even so, the local compression stresses are acceptable, considering the short time load' nature. An opinion concerning possible remnant deformations will be expressed after the results of a new and detailed geotechnical study on site.

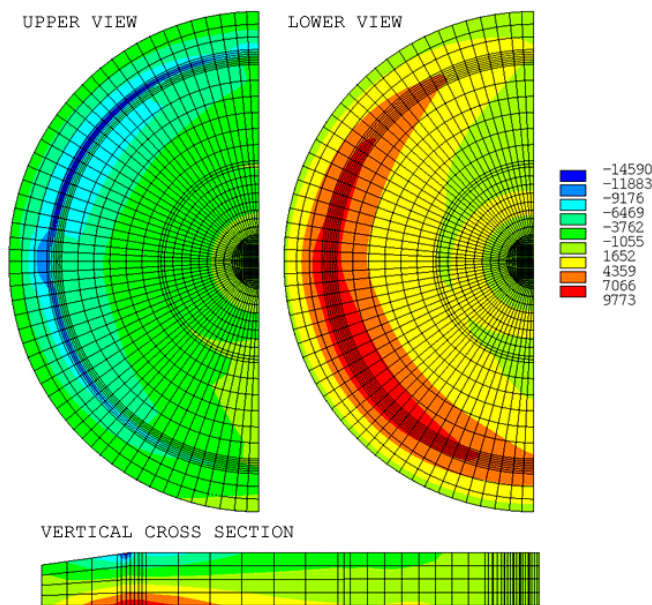


Fig. 30 – Combination [ST]–[EQY]–[EQX] – radial stress distribution in the foundation slab (KN/m<sup>2</sup>).

## 15. Concluding remarks

The results obtained by modeling the spatial interaction of the soil-structure assembly in both stages of the analysis show a significant influence on the structural state of stress and deformation. Despite the axial symmetric shape of the structure, it was demonstrated in both static and dynamic load conditions that the load transmission to the ground through the foundation slab depends on the deformability of the soil mass. The more the ground is deformable, the more a larger fraction of the vertical load is transferred toward the exterior cylindrical plate, to the detriment of the central region of the foundation slab.

From the point of view of stress distribution, interaction proves to be a complex phenomenon. Generally, modeling the deformability of supports reduces the structural stresses, compared with the embedded situation. On the other hand, the ground deformability induces second order effects, augmenting the horizontal load effect ( $P - \Delta$ ). In the peculiar case, a redistribution of stresses between the structural components occurs. The fact is not necessarily determined by the seismic load, but of those due to in-duty conditions, which have the major weight in the load case combination.

## References

- [1]. Prişcu R., Stematiu D., (1980). *Ingineria seismică a construcțiilor hidrotehnice, Chapter 4. Reservoirs, Elevated Water Tanks, Intake Towers*. Bucureşti: Ed. Didactică și Pedagogică.
- [2]. Eurocode 8 EN. (1998). 4: 2006